Soft Matter

PAPER

View Article Online
View Journal | View Issue

Check for updates

Cite this: *Soft Matter*, 2023, **19**, 1131

Diffusiophoresis of a spherical particle in porous media

Siddharth Sambamoorthy and Henry C. W. Chu *

Received 9th December 2022,
Accepted 15th January 2023

DOI: 10.1039/d2sm01620f

rsc.li/soft-matter-journal

Published on 17 2023. Downloaded on 02.11.2024 23:21:51.

Recent experiments by Doan *et al.* (*Nano Lett.*, 2021, **21**, 7625–7630) demonstrated and measured colloid diffusiophoresis in porous media but existing theories cannot predict the observed colloid motion. Here, using regular perturbation method, we develop a mathematical model that can predict the diffusiophoretic motion of a charged colloidal particle driven by a binary monovalent electrolyte concentration gradient in a porous medium. The porous medium is modeled as a Brinkman medium with a constant Darcy permeability. The linearized Poisson–Boltzmann equation is employed to model the equilibrium electric potential distribution that is driven out-of-equilibrium under diffusiophoresis. We report three key findings. First, we demonstrate that colloid diffusiophoresis could be drastically hindered in a porous medium due to the additional hydrodynamic drag compared to diffusiophoresis in a free electrolyte solution. Second, we show that the variation of the diffusiophoretic motion with respect to a change in the electrolyte concentration in a porous medium could be qualitatively different from that in a free electrolyte solution. Third, our results match quantitatively with experimental measurements, highlighting the predictive power of the present model. The mathematical model developed here could be employed to design diffusiophoretic colloid transport in porous media, which are central to applications such as nanoparticle drug delivery and enhanced oil recovery.

1 Introduction

Diffusiophoresis is the deterministic motion of particles induced by a surrounding concentration gradient of solutes.[1–4] Diffusiophoresis comprises an electrophoretic component due to the electric field induced by a disparity in the diffusivities of the ionic solutes, and a chemiphoretic component due to the osmotic pressure gradient associated with the solute concentration gradient. Motivated by manufacturing colloidal coatings for vehicles, Prieve *et al.*[5,6] pioneered a theory to predict the diffusiophoretic motion of a colloidal particle in a concentration gradient of electrolytes, the so-called log-sensing relation $\boldsymbol{U} = M\nabla \log n$, where the mobility M relates the particle diffusiophoretic velocity $\boldsymbol{U}$ and gradient of the natural logarithm of the solute concentration n. Since then, much work has been done to characterize the diffusiophoretic mobility of rigid particles in various solutes,[7–12] the mobility of drops and soft particles,[13–20] and the mobility in confined environments.[21–23] In addition to develop fundamental theories for diffusiophoresis, progress has been made in devising new applications using diffusiophoresis, ranging from mixing and separation of colloids,[9,24–40] enhanced oil recovery,[41–43] drug delivery,[44,45] to water and surface cleaning.[46–48] The strengths of diffusiophoresis are prominent in two aspects. First, diffusiophoresis can generate a significant colloid motion on the microscale. For instance, the diffusivity of a typical ionic solute $D \sim M \sim 10^{-9}$ m s^{-2} and the length of the solute gradient $L \sim n/\nabla n \sim \lessapprox 10^{-3}$ m, giving $U \gtrapprox 10^{-6}$ m s^{-1}. Second, diffusiophoresis can transport colloids into dead-end pores,[49–51] which cannot be achieved by traditional means such as pressure pumping due to the zero volumetric fluid flow in the pore by conservation of mass.

However, the majority of work in the literature focuses on diffusiophoresis in a free electrolyte solution and a theory for predicting colloid diffusiophoresis in an electrolyte-filled porous medium is lacking. Porous media are ubiquitous in artificial and natural settings. For instance, tumor interstitia are filled with biohydrogels which hinder nanoparticle drug delivery.[44,52,53] Distinct from transport in a free electrolyte solution, colloids experience friction and retardation as they travel through a porous medium. As a proof of concept of a novel nanoparticle drug delivery protocol in biological systems, recently Doan *et al.*[45] demonstrated and measured diffusiophoresis of nanoparticles in a porous hydrogel. Specifically, they constructed microfluidic dead-end pores filled with collagen hydrogel and an electrolyte solution, mimicking tumor interstitia. They then generated an electrolyte concentration gradient across the dead-end pores by flowing an electrolyte solution of a different concentration past the opening of the pores. Because of the high aspect ratio of the dead-end pores,

Department of Chemical Engineering, University of Florida, Gainesville, FL 32611, USA. E-mail: h.chu@ufl.edu

Published on 17 2023. Downloaded on 02.11.2024 23:21:51.

they assumed that the nanoparticle displacement $x(t)$ and electrolyte concentration field $n(x,t)$ are one-dimensional and follow the integrated log-sensing relation, $x(t) = \int M \nabla \log n(x,t) \mathrm{d}t$. They extracted the mobility by fitting this relation to a theoretically deduced $n(x,t)$ and an experimentally measured $x(t)$.

Despite the success in inferring the mobility, the experiment[45] suffers from several drawbacks. First, it requires tracking the nanoparticle displacement which is subject to thermal fluctuations and demands averaging over multiple experiments to minimize statistical errors. Second, it requires a long time (up to days) to prepare the gel- and electrolyte-filled dead-end pores and to observe sufficiently large nanoparticle displacements for inferring the mobility. Third, and most importantly, the experiments cannot predict the particle diffusiophoretic motion (mobility). Hence, there is a need for a predictive theory for the colloid diffusiophoretic mobility in a porous medium, analogous to that for colloid diffusiophoresis in a free electrolyte solution.[6]

In this work, we develop a mathematical model that can predict the diffusiophoretic colloid mobility in a porous medium. The model considers a charged colloidal particle undergoing diffusiophoresis in a porous medium subject to a spatially uniform concentration gradient of a binary monovalent electrolyte. We invoke the Debye–Huckel approximation, which is accurate to model the electric potential of a charged particle in many practical cases, where $\phi \leq 50\,\mathrm{mV}$ at room temperature.[54] To account for the frictional force exerted by the porous network on the fluid and particle motion, the porous medium is modeled as a Brinkman medium[55] with a constant Darcy permeability. We report three key findings. First, we show that, compared to diffusiophoresis in a free electrolyte solution, colloid diffusiophoresis could be significantly hampered in porous media due to friction, as reflected in a decrease in the magnitude of the mobility. Second, we demonstrate that the variation of the mobility with electrolyte concentration could be altered qualitatively by the presence of porous media. Third, our model predictions make quantitative agreements with experiments[45] with no fitting parameters.

The rest of this article is outlined as follows. In Section 2, we formulate the problem by first presenting the governing equations and boundary conditions for the fluid and ion transport as well as the electric potential distribution of the charged colloidal particle and the surrounding electrolyte-filled porous media. Then, we conduct a regular perturbation in the imposed electrolyte concentration gradient to obtain a set of ordinary differential equations that determine the diffusiophoretic mobility of the particle. In Section 3, we present our results and elaborate on the three above-mentioned key findings. In Section 4, we summarize this study and offer ideas for future work.

2 Problem formulation

Consider a non-conducting particle of radius a and constant surface charge q (or constant surface potential ζ) in a static porous medium with a constant Darcy permeability l^2 (l is the Brinkman screening length), subject to a spatially uniform concentration gradient of a binary monovalent electrolyte ∇n_i^∞, where $i = 1$ and $i = 2$ are the cationic and anionic species, respectively (Fig. 1). Due to symmetry, the particle translates with a constant diffusiophoretic velocity $\boldsymbol{U}$ parallel to ∇n_i^∞ along the z-direction. The velocity $\boldsymbol{U}$ is an unknown to be determined. A reference frame moving with $\boldsymbol{U}$ is adopted.

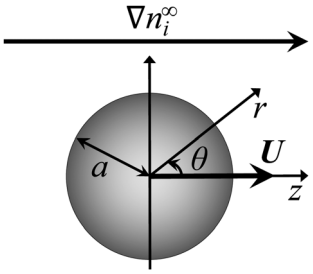

Fig. 1 A concentration gradient ∇n_i^∞ of ionic species i induces diffusiophoretic motion of a particle of radius a in a static porous medium. The diffusiophoretic velocity of the particle $\boldsymbol{U}$ is parallel to ∇n_i^∞.

In the steady state, conservation of individual species requires that

$$\nabla \cdot \boldsymbol{j}_i = 0 \quad \text{with } \boldsymbol{j}_i = -D_i \nabla n_i - \frac{D_i z_i e}{kT} n_i \nabla \phi + n_i \boldsymbol{u}, \tag{1}$$

where $\boldsymbol{j}_i$, D_i, and z_i (with $z_1 = -z_2 = 1$) are the flux density, diffusivity, and valence of the i-species, respectively; e is the charge on a proton, k is the Boltzmann constant, T is the absolute temperature, ϕ is the electric potential, and $\boldsymbol{u}$ is velocity of the electrolyte solution. The electric potential satisfies the Poisson equation

$$-\varepsilon \nabla^2 \phi = \rho = z_1 e n_1 + z_2 e n_2, \tag{2}$$

where ε and ρ are the permittivity and space charge density of the electrolyte solution, respectively. Inertial forces are negligible in colloidal-scale transport. The fluid dynamics is described by the continuity equation in addition to the Brinkman equation with an electric body force[56–58]

$$\nabla \cdot \boldsymbol{u} = 0 \quad \boldsymbol{0} = -\nabla p + \eta \nabla^2 \boldsymbol{u} - \rho \nabla \phi - \eta l^{-2} (\boldsymbol{u} + \boldsymbol{U}), \tag{3}$$

where p is the pressure and η is the dynamic viscosity of the electrolyte solution. The last term in eqn (3) accounts for the frictional force exerted by the porous medium on the fluid.

To specify the problem, eqn (1)–(3) should be accompanied with boundary conditions at the particle surface and at location far from the particle. At the particle surface, $r = a$, no hydrodynamic slip and no penetration of the solvent require that

$$\boldsymbol{u} = \boldsymbol{0}. \tag{4}$$

No penetration of the ionic species requires that

$$\boldsymbol{n} \cdot \boldsymbol{j}_i = 0, \tag{5}$$

where $\boldsymbol{n}$ is the unit normal vector pointing away from the particle surface. The surface charge q or the surface potential ζ of the particle could be specified, respectively, *via*

$$-\boldsymbol{n} \cdot \varepsilon \nabla \phi = q \quad \text{or } \phi = \zeta. \tag{6}$$

 This journal is © The Royal Society of Chemistry 2023

Published on 17 2023. Downloaded on 02.11.2024 23:21:51.

At location far from the particle, $r \to \infty$, it requires that

$$\boldsymbol{u} \to -\boldsymbol{U} \quad \text{and} \quad p \to p^{\infty}, \tag{7}$$

where p^{∞} is a reference constant pressure. The electrolyte concentration field and its gradient are represented by a truncated Taylor series

$$n_i \to n_i^{\infty} + \nabla n_i^{\infty} \cdot \boldsymbol{r}, \tag{8}$$

where n_i^{∞} is the uniform electrolyte concentration in the bulk and $\nabla n_i^{\infty} \cdot \boldsymbol{r}$ is associated with the spatially uniform electrolyte concentration gradient. The position vector $\boldsymbol{r}$ is anchored at the centroid of the particle. The electrolyte concentration gradient induces an electric potential gradient to maintain bulk electroneutrality[6,59]

$$-\nabla\phi = \frac{kT}{e}\beta\mathbf{G}, \tag{9}$$

where $\boldsymbol{G} = (\nabla n_1^{\infty})/n_1^{\infty} = (\nabla n_2^{\infty})/n_2^{\infty}$ and $\beta = (D_1 - D_2)/(D_1 + D_2)$.

We linearize eqn (1)–(9) to probe typical regimes of diffusiophoresis, where the electrolyte gradient at the size of the particle is much smaller than the background concentration. To this end, we define a small parameter $\alpha = |\boldsymbol{G}|a \ll 1$ and perform a regular perturbation analysis for the dependent variables

$$\begin{aligned} &n_i = n^{\infty}\left(\hat{n}_i^0 + \alpha\hat{n}_i^1\right), \quad \phi = \frac{kT}{e}\left(\hat{\phi}^0 + \alpha\hat{\phi}^1\right), \\ &\boldsymbol{u} = \frac{\varepsilon k^2T^2}{e^2\eta a}\left(\hat{\boldsymbol{u}}^0 + \alpha\hat{\boldsymbol{u}}^1\right), \quad p = \frac{\varepsilon k^2T^2}{e^2a^2}\left(\hat{p}^0 + \alpha\hat{p}^1\right), \end{aligned} \tag{10}$$

where $n^{\infty} = 2I = {z_1}^2 n_1^{\infty} + {z_2}^2 n_2^{\infty}$ is twice the ionic strength of the electrolyte. In eqn (10), quantities with carets are dimensionless and the factors outside the brackets are the dimensional groups for non-dimensionalizing the left-hand side of the equation, *e.g.*, n_i/n^{∞} is dimensionless. Lengths are non-dimensionalized by the particle radius a. Substituting eqn (10) into eqn (1)–(9) furnishes a set of differential equations at different order of α. In the following, we begin with the leading order [$O(1)$] perturbation and will arrive at a set of equations for computing the diffusiophoretic velocity (mobility) at the $O(\alpha)$ perturbation. Hereafter, carets are dropped for clarity unless specified otherwise.

2.1 Leading order perturbation

The leading order perturbation concerns the equilibrium condition where there is no electrolyte concentration gradient and therefore no fluid flow, $\boldsymbol{u}^0 = \boldsymbol{0}$. In other words, the momentum eqn (3) does not provide useful information at the leading order perturbation. Hence, only the perturbed eqn (1) and (2) and their boundary conditions are presented below.

The leading order ion conservation and Poisson equation are

$$\nabla\cdot\left(-\nabla n_i^0 - z_i n_i^0 \nabla\phi^0\right) = 0, \tag{11}$$

$$\nabla^2\phi^0 = -(\kappa a)^2\left(z_1 n_1^0 + z_2 n_2^0\right), \tag{12}$$

where the Debye length $\kappa^{-1} \equiv (\varepsilon kT/e^2 n^{\infty})^{1/2}$ is the length scale over which the space charge density varies. The leading order boundary conditions at the particle surface, $r = 1$, are

$$\boldsymbol{n}\cdot\left(-\nabla n_i^0 - z_i n_i^0 \nabla\phi^0\right) = 0, \tag{13}$$

$$-\boldsymbol{n}\cdot\nabla\phi^0 = \frac{qea}{\varepsilon kT} \equiv \hat{q} \quad \text{or} \quad \phi^0 = \frac{\zeta e}{kT} \equiv \hat{\zeta}, \tag{14}$$

where $\hat{q}$ and $\hat{\zeta}$ denote the non-dimensionalized particle surface charge and surface potential, respectively. The leading order boundary conditions far from the particle, $r \to \infty$, are

$$n_i^0 \to n_i^{\infty} \quad \text{and} \quad \phi^0 \to 0. \tag{15}$$

Integrating eqn (11) and applying eqn (15) yields the Boltzmann distribution of the ionic species, $n_i^0 = n_i^{\infty}\exp(-z_i\phi^0)$. Substituting this result in eqn (12) furnishes the nonlinear Poisson–Boltzmann equation, which can be linearized using the Debye–Huckel approximation as $\nabla^2\phi^0 = (\kappa a)^2\phi^0$. Utilizing eqn (14) and (15), the spherically symmetric equilibrium electric potential for a particle with a constant surface charge or a constant surface potential can be obtained, respectively, as

$$\phi^0 = \frac{\hat{q}\exp[-\kappa a(r-1)]}{(\kappa a+1)r} \quad \text{or} \quad \phi^0 = \frac{\hat{\zeta}\exp[-\kappa a(r-1)]}{r}, \tag{16}$$

which establish a relation between the non-dimensionalized particle surface potential and surface charge as

$$\hat{\zeta} = \frac{\hat{q}}{\kappa a + 1}. \tag{17}$$

2.2 $O(\alpha)$ perturbation

The $O(\alpha)$ equations can be simplified and converted to a set of ordinary differential equations by introducing the ψ_i^1 potential, $n_i^1 = -z_i n_i^0(\psi_i^1 + \phi^1)$,[60] and exploiting symmetry of the problem to write the dependent variables as[61]

$$\begin{aligned} &u_r^1(r,\theta) = -\frac{2}{r}h\cos\theta, \quad u_\theta^1(r,\theta) = \frac{1}{r}\frac{\mathrm{d}(rh)}{\mathrm{d}r}\sin\theta, \\ &\psi_i^1(r,\theta) = \Psi_i^1\cos\theta, \end{aligned} \tag{18}$$

where u_r^1 and u_θ^1 are the radial and angular components of $\boldsymbol{u}^1$. The $O(\alpha)$ problem now requires solving for $h = h(r)$ and $\Psi_i^1 = \Psi_i^1(r)$, which are governed by

$$\frac{\mathrm{d}^2\Psi_i^1}{\mathrm{d}r^2} + \frac{2}{r}\frac{\mathrm{d}\Psi_i^1}{\mathrm{d}r} - \frac{2}{r^2}\Psi_i^1 - z_i\frac{\mathrm{d}\phi^0}{\mathrm{d}r}\frac{\mathrm{d}\Psi_i^1}{\mathrm{d}r} + 2\frac{\mathrm{Pe}}{D_i}\frac{\mathrm{d}\phi^0}{\mathrm{d}r}\frac{h}{r} = 0, \tag{19}$$

$$\begin{aligned} &\frac{\mathrm{d}^4h}{\mathrm{d}r^4} + \frac{4}{r}\frac{\mathrm{d}^3h}{\mathrm{d}r^3} - \frac{4}{r^2}\frac{\mathrm{d}^2h}{\mathrm{d}r^2} - \left(\frac{a}{l}\right)^2\left(-\frac{2}{r^2}h + \frac{2}{r}\frac{\mathrm{d}h}{\mathrm{d}r} + \frac{\mathrm{d}^2h}{\mathrm{d}r^2}\right) \\ &+ \frac{(a\kappa)^2}{r}\frac{\mathrm{d}\phi^0}{\mathrm{d}r}\left({z_1}^2 n_1^0\Psi_1^1 + {z_2}^2 n_2^0\Psi_2^1\right) = 0, \end{aligned} \tag{20}$$

where the Peclet number $\mathrm{Pe} \equiv \varepsilon k^2T^2/(\eta e^2 D_s)$ describes the ratio of advective to diffusive contributions to ion transport, with D_s being the diffusivity scale and chosen as the cation diffusivity.

Published on 17 2023. Downloaded on 02.11.2024 23:21:51.

The $O(\alpha)$ boundary conditions at the particle surface, $r = 1$, are

$$\frac{\mathrm{d}\Psi_i^1}{\mathrm{d}r} = 0, \quad h = 0, \quad \frac{\mathrm{d}h}{\mathrm{d}r} = 0. \tag{21}$$

The $O(\alpha)$ boundary conditions far from the particle, $r \to \infty$, are

$$\Psi_1^1 \to (\beta - 1)r, \quad \Psi_2^1 \to (\beta + 1)r, \tag{22}$$

$$h \to \frac{1}{2}\mu r, \tag{23}$$

where μ is the non-dimensionalized diffusiophoretic mobility and relates to the dimensional diffusiophoretic mobility M *via*

$$\mu = \frac{U}{\alpha} = \frac{e^2\eta}{\varepsilon k^2 T^2} M. \tag{24}$$

Eqn (22) and (23) are set at $r \to \infty$. To have a well-defined boundary value problem in a finite domain, we follow prior work[59,60] and set the computational domain to a sphere of radius R which is concentric to the particle and completely encloses the particle. At a sufficiently large R, the electric potential decays to zero asymptotically as $(1/r)\exp(-\kappa a r)$. A value $R = 1 + 20/(\kappa a)$ suffices. We solve eqn (19) in this asymptotic limit, where terms associated with derivatives of ϕ^0 vanish, and obtain the following expressions in replacement of eqn (22)

$$2\Psi_1^1 + R\frac{\mathrm{d}\Psi_1^1}{\mathrm{d}r} = 3(\beta - 1)R, \quad 2\Psi_2^1 + R\frac{\mathrm{d}\Psi_2^1}{\mathrm{d}r} = 3(\beta + 1)R. \tag{25}$$

For a freely suspended particle, the net hydrodynamic and electric force is zero on the large sphere of radius R. A sufficiently large R guarantees that the sphere is electric force-free. Thus, the constraint here reduces to that the sphere of radius R should be hydrodynamic force-free

$$\boldsymbol{F} = 2\pi R^2 \int_0^\pi \boldsymbol{\sigma} \cdot \boldsymbol{n} \, \sin\theta \mathrm{d}\theta = 0, \tag{26}$$

where $\boldsymbol{\sigma} = -p\boldsymbol{I} + \eta(\nabla\boldsymbol{u} + (\nabla\boldsymbol{u})^T)$ is the Newtonian stress tensor and $\boldsymbol{I}$ is the identity tensor. Solving eqn (20) in the asymptotic limit of vanishing electric potential along with eqn (26) gives

$$\begin{aligned} &R^2\left(R^2\gamma^2 + 3R\gamma + 3\right)\frac{\mathrm{d}^2 h}{\mathrm{d}r^2} \\ &\quad + \left(R^3\gamma^3 + 3R^2\gamma^2 + 6R\gamma + 6\right)\left(R\frac{\mathrm{d}h}{\mathrm{d}r} - h\right) \\ &\quad = 0 \end{aligned} \tag{27}$$

$$\begin{aligned} &\left(R^2\gamma^2 + 3R\gamma + 3\right)\left[R^2\frac{\mathrm{d}^3 h}{\mathrm{d}r^3} + R(R\gamma + 4)\frac{\mathrm{d}^2 h}{\mathrm{d}r^2}\right] \\ &\quad + 3\gamma\left(R^2\gamma^2 + 2R\gamma + 2\right)\left(R\frac{\mathrm{d}h}{\mathrm{d}r} - h\right) = 0, \end{aligned} \tag{28}$$

$$\frac{3}{2}\mu = \frac{3(R\gamma + 1)}{R^2\gamma^2 + 3R\gamma + 3}\frac{\mathrm{d}h}{\mathrm{d}r} + \frac{3\left(R^2\gamma^2 + 2R\gamma + 2\right)}{R^2\gamma^2 + 3R\gamma + 3}\frac{h}{R}, \tag{29}$$

where $\gamma = a/l$. Eqn (27) and (28) replace (23). In sum, we solve eqn (19) and (20) subject to eqn (25), (27) and (28) for h and Ψ_i^1 using the built-in solver *NDSolve* in Wolfram Mathematica. The diffusiophoretic mobility could be obtained from eqn (29). In the limit $\gamma \to 0$, these equations recover those for particle diffusiophoresis in a free electrolyte solution.[59]

3 Results and discussion

In this section, we present the diffusiophoretic mobility of a particle in porous media filled with an electrolyte solution. In Section 3.1, we present results for porous media filled with potassium chloride (KCl) solution. Note that electrophoresis is negligible in a KCl solution due to the small diffusivity ratio, $\beta = -0.02$. Thus, we follow prior work[18,59,62,63] and assume $\beta = 0$ so that diffusiophoresis is solely due to chemiphoresis. This enables understanding of chemiphoresis in porous media. In Section 3.2, we present results for porous media filled with sodium chloride (NaCl) solution, which has a large diffusivity ratio, $\beta = -0.21$. Both electrophoresis and chemiphoresis contribute significantly to particle diffusiophoresis. In Section 3.3, we compare our modeling predictions with experiments.

3.1 Diffusiophoresis in porous media with KCl solution

Let us start by examining colloid diffusiophoresis in porous media filled with a KCl solution. Fig. 2 shows the variation of the non-dimensionalized diffusiophoretic mobility with the non-dimensionalized particle surface potential for different ratios of the Brinkman screening length to particle radius, l/a. The ratio of the particle radius to Debye length is set as $\kappa a = 10$. Physically, l/a can be interpreted as a permeability parameter. Namely, a large $l/a(\gg 1)$ represents a free electrolyte solution whereas a small $l/a(\ll 1)$ represents a weakly permeable porous medium filled with the electrolyte. As an overview of the figure, the mobility is positive, meaning that the particle is driven up the electrolyte concentration gradient under chemiphoresis. This is because the imposed electrolyte gradient

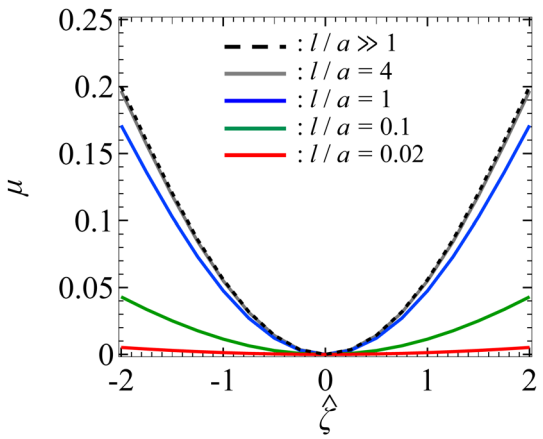

Fig. 2 Diffusiophoresis in porous media with potassium chloride solution where $\beta = 0$. Variation of the non-dimensionalized diffusiophoretic mobility μ with the non-dimensionalized particle surface potential $\hat{\zeta}$ for different ratios of Brinkman screening length to particle radius l/a. The ratio of particle radius to Debye length $\kappa a = 10$. Dashed line: a free electrolyte solution where $l/a \gg 1$. Solid lines: electrolyte-filled porous media of different l/a.

This journal is © The Royal Society of Chemistry 2023

Published on 17 2023. Downloaded on 02.11.2024 23:21:51.

generates a chemiosmotic flow over the particle surface from region of high to low electrolyte concentration, and the particle is moving in the opposite direction under chemiphoresis.[1–4]

In Fig. 2, the dashed line recovers the particle mobility in a free electrolyte solution.[18,59] The mobility is symmetric with respect to the sign of the particle surface potential, which is due to the absence of electrophoresis. The solid lines show the mobility in porous media with different permeabilities. The mobility is still an even function of the particle surface potential, since electrophoresis is still absent. Also, at a fixed $\hat{\zeta}$, the mobility decreases as l/a decreases. This could be understood as follows. Lowering l/a implies a lower permeability of the electrolyte solution in the porous medium. Thus, there is a weaker chemiosmotic flow past the particle and, consequently, particle chemiphoresis is weakened as reflected in a smaller particle mobility. Alternatively, one could understand this observation by recognizing that the porous medium introduces additional hydrodynamic drag to the particle, which scales as $(a/l)^2$,[55,64] as shown in eqn (20). Thus, decreasing l/a lowers the mobility.

Next, Fig. 3(a) shows the variation of the non-dimensionalized diffusiophoretic mobility with κa for different l/a. The non-dimensionalized particle surface potential $\hat{\zeta} = -1$. As an overview of the figure, a line of fixed l/a can be interpreted as fixing the permeability of the porous medium, l, and the size of the particle, a. Thus, at a fixed l/a, increasing κa implies increasing κ, which can be achieved in practice by increasing the bulk electrolyte concentration n^∞ (recall that $\kappa \sim \sqrt{n^\infty}$).

In Fig. 3(a), the dashed line recovers the particle mobility in a free electrolyte solution.[18,59] The mobility increases as κa

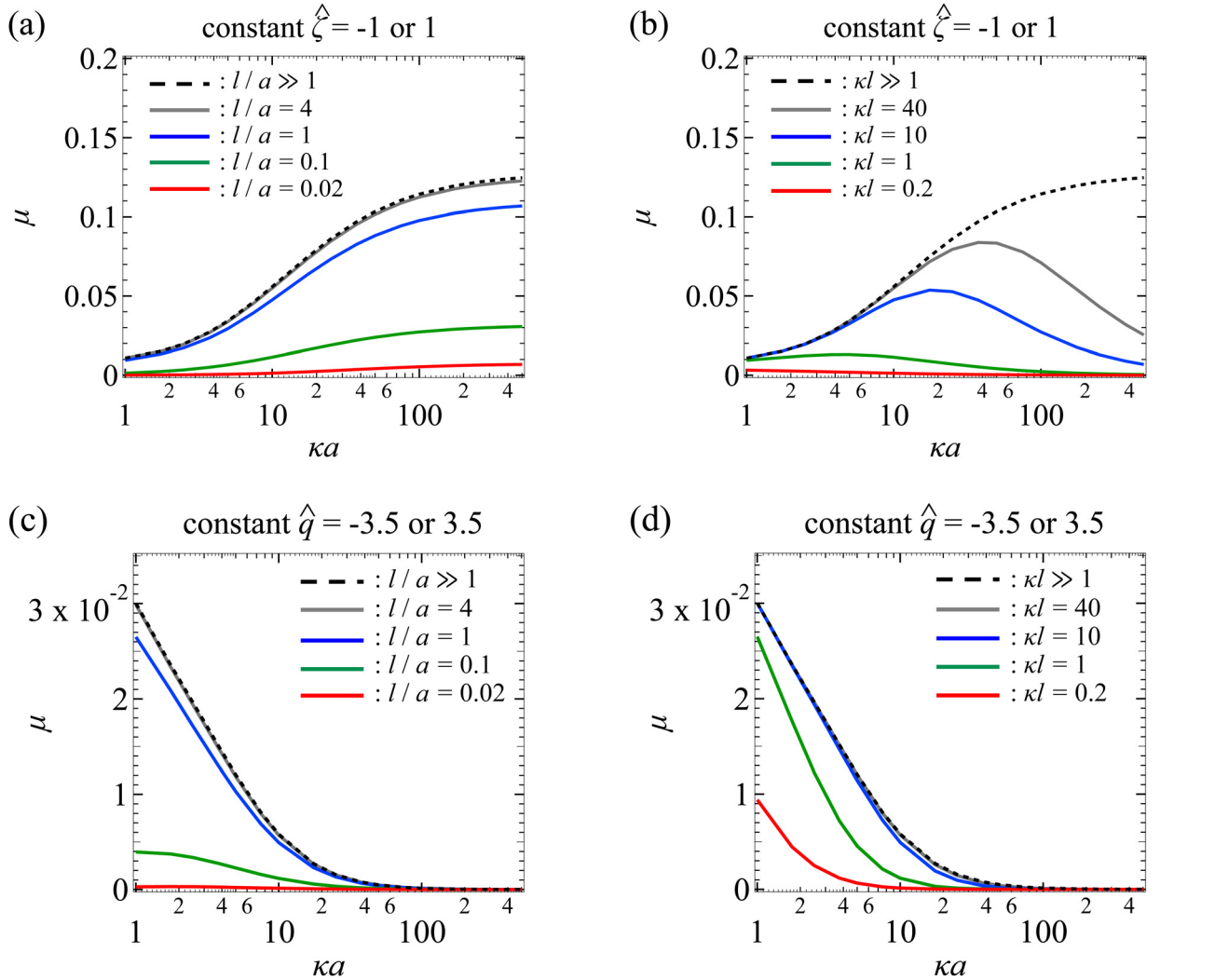

Fig. 3 Diffusiophoresis in porous media with potassium chloride solution where $\beta = 0$. (a) Variation of the non-dimensionalized diffusiophoretic mobility μ with the ratio of particle radius to Debye length κa for different ratios of Brinkman screening length to particle radius l/a. Results are the same for the non-dimensionalized particle surface potential $\hat{\zeta} = -1$ or 1. Dashed line: a free electrolyte solution where $l/a \gg 1$. Solid lines: electrolyte-filled porous media of different l/a. (b) Variation of μ with κa for different ratios of Brinkman screening length to Debye length κl. Results are the same for $\hat{\zeta} = -1$ or -1. Dashed line: a free electrolyte solution where $\kappa l \gg 1$. Solid lines: electrolyte-filled porous media of different κl. Parameters used in (c) and (d) are the same as (a) and (b), respectively, except that the non-dimensionalized particle surface charge is fixed, $\hat{q} = -3.5$ or 3.5 where their results are the same, instead of the surface potential.

Published on 17 2023. Downloaded on 02.11.2024 23:21:51.

increases. This is because, as noted in the above paragraph, increasing κa implies an increasing bulk ion concentration. Hence, there are more ions that contribute to a stronger chemiosmotic flow and therefore stronger chemiphoresis, as reflected in a larger mobility. The mobility plateaus as $\kappa a \gg 1$, since the chemiosmotic flux saturates in the limit of a vanishingly thin electric double layer. The solid lines show the mobility in porous media with different permeabilities. At a fixed κa, the mobility decreases as l/a decreases, consistent with the explanation provided in Fig. 2. On a different note, we have conducted separate computations and confirmed that the mobility of a particle with a constant surface potential $\hat{\zeta}$;= 1 is the same as that shown in Fig. 3(a) for $\hat{\zeta} = -1$. This is again due to the absence of electrophoresis.

Fig. 3(b) shows the variation of the non-dimensionalized diffusiophoretic mobility with κa for different ratios of the Brinkman screening length to Debye length κl. The non-dimensionalized particle surface potential $\hat{\zeta} = -1$. As an overview of the figure, a line of fixed κl can be interpreted as fixing the permeability of the porous medium, l, and the concentration of the solution, κ. Thus, at a fixed κl, increasing κa implies increasing the particle radius a, which can be achieved in practice by using particles of different sizes. The dashed line recovers the particle mobility in a free electrolyte solution.[18,59]

In Fig. 3(b), the solid lines show the mobility in porous media with different κl. For $\kappa l \geq 1$, the mobility first increases and then decreases with increasing κa, distinct from the response in a free electrolyte solution. To understand this non-monotonic response, let us consider the (grey) line with $\kappa l = 40$ as an example. Before the mobility rises to a peak, the particle radius, a, is small compared to the mesh size of the porous medium ($\sim l$). For instance, at $\kappa a = 10$, $a/l = 1/4$. Physically, the hindrance due to the porous medium is not felt by the particle. The resulting reduction in mobility is insignificant compared to the enhancement to the mobility due to increasing κa. Thus, before attaining the peak which corresponds to $a/l \sim O(1)$, the mobility increases with increasing κa. Beyond the peak where $a/l > O(1)$, the mobility decreases with increasing κa. This is because the hindrance due to the porous medium outweighs the enhancement due to increasing κa, leading to an overall decrease in the mobility as κa increases.

In Fig. 3(b), a peak is not exhibited for $\kappa l < 1$ (red line). This is because $a/l > O(1)$ for the entire range of κa shown in the figure. Thus, the hindrance due to the porous medium and the resulting reduction in mobility dominate the enhancement due to increasing κa. On a different note, at a fixed κa, lowering κl decreases the mobility. This is because lowering κl at a fixed κa implies lowering l/a, which increases the hydrodynamic drag to the particle and thus lowers the mobility, as explained in Fig. 2. As an additional remark, we have conducted separate computations and confirmed that the mobility of a particle with a constant surface potential $\hat{\zeta} = 1$ is identical to that shown in Fig. 3(b) for $\hat{\zeta} = -1$.

Next, let us turn our focus to Fig. 3(c) which shows the variation of the non-dimensionalized diffusiophoretic mobility with κa for different l/a. Here, the non-dimensionalized particle surface charge is fixed $\hat{q} = -3.5$ instead of the surface potential. Particles of a constant surface charge are more practically relevant in some cases,[63,65,66] although prior work has focused on particles of a constant surface potential.[8,18,20,59,62] For a particle with a constant surface charge, its surface potential decreases with increasing κa [eqn (17)]. In Fig. 3(c), the maximum non-dimensionalized potential $|\hat{\zeta}| = 1.7$ occurs at $\kappa a = 1$, which justifies the use of the Debye–Huckel approximation to compute the electric potential accurately.[54]

In Fig. 3(c), the dashed line shows the particle mobility in a free electrolyte solution. Going from top to bottom of the figure, at a fixed κa, the mobility decreases as l/a decreases, which is consistent with the explanation given in Fig. 2. Going from left to right of the figure, for a line of constant l/a, the mobility is maximum when κa is the smallest and decreases to zero on approaching the limit $\kappa a \gg 1$. This trend follows from the relation between the particle surface charge and surface potential [eqn (17)], where the latter vanishes in the limit of $\kappa a \gg 1$ and so does the mobility. On a different note, we have conducted separate computations and confirmed that the mobility of a particle with a constant surface charge $\hat{q} = 3.5$ is identical to that shown in Fig. 3(c) for $\hat{q} = -3.5$.

Next, let us look at Fig. 3(d) that shows the variation of the non-dimensionalized diffusiophoretic mobility with κa for different κl. The non-dimensionalized particle surface charge $\hat{q} = -3.5$. The dashed line shows the particle mobility in a free electrolyte solution. Going from top to bottom of the figure, at a fixed κa, the mobility decreases as l/a decreases, which is consistent with the explanation provided in Fig. 2. Going from left to right of the figure, for a line of constant l/a, the mobility decreases from a maximum when κa is the smallest to zero on approaching the limit $\kappa a \gg 1$. We have conducted separate computations and confirmed that the mobility of a particle with a constant surface charge $\hat{q} = 3.5$ is the same as that shown in Fig. 3(d) for $\hat{q} = -3.5$.

3.2 Diffusiophoresis in porous media with NaCl solution

Let us turn to examine colloid diffusiophoresis in porous media filled with a NaCl solution. Fig. 4 shows the variation of the non-dimensionalized diffusiophoretic mobility with the non-dimensionalized particle surface potential for different l/a and $\kappa a = 10$. The dashed line recovers the particle mobility in a free electrolyte solution.[18,59] Distinct from Fig. 2 for KCl solution, here the particle mobility in a NaCl solution is asymmetric with respect to the sign of the particle surface potential due to the presence of electrophoresis. Specifically, because of the difference in the diffusivity between the sodium and chloride ions, an electric field is induced to maintain bulk electroneutrality in the imposed electrolyte gradient. This electric field induces electrophoretic motion of the particle, where a negatively (positively) charged particle is driven up (down) the electrolyte gradient. However, chemiphoresis is also present and it drives a particle up the electrolyte gradient, regardless of the sign of the particle surface potential. Hence, electrophoresis and chemiphoresis are both driving a negatively charged particle up the electrolyte gradient whereas they are acting in the opposite

 This journal is © The Royal Society of Chemistry 2023

Published on 17 2023. Downloaded on 02.11.2024 23:21:51.

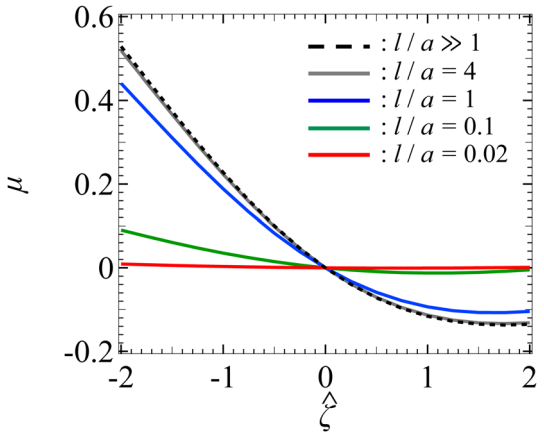

Fig. 4 Diffusiophoresis in porous media with sodium chloride solution where $\beta = -0.21$. Variation of the non-dimensionalized diffusiophoretic mobility μ with the non-dimensionalized particle surface potential $\hat{\zeta}$ for different ratios of Brinkman screening length to particle radius l/a. The ratio of particle radius to Debye length $\kappa a = 10$. Dashed line: a free electrolyte solution where $l/a \gg 1$. Solid lines: electrolyte-filled porous media of different l/a.

direction on a positively charged particle. As a result, for a positively charged particle where electrophoresis outweighs chemiphoresis, the particle is driven down the electrolyte gradient as reflected in a negative mobility. In contrast, for a negatively charged particle, the mobility is positive and has a larger magnitude compared to a positively charged particle that has the same magnitude of surface potential.

In Fig. 4, the solid lines show the mobility in porous media with different permeabilities. At a fixed $\hat{\zeta}$, the magnitude of the mobility decreases as l/a decreases. This aligns with the explanation given in Fig. 2, where a small l/a implies a low permeability of the electrolyte solution in the porous medium. Hence, there is a weaker chemiosmotic and electroosmotic flow past the particle. As a result, particle diffusiophoresis is weakened as reflected in a smaller particle mobility. Also, the asymmetry of the mobility with respect to the sign of the particle surface potential persists in the presence of a porous medium. This implies that varying the permeability of the porous medium only impacts the magnitude of the particle diffusiophoretic motion but not its direction.

Fig. 5(a) shows the variation of the non-dimensionalized diffusiophoretic mobility with κa for different l/a. Let us first examine the upper quadrant of the figure, which corresponds to a particle with a constant non-dimensionalized surface potential $\hat{\zeta} = -1$. Recall that the diffusiophoretic mobility comprises the chemiphoretic and electrophoretic component and, from Fig. 4, they both drive a negatively charged particle up the electrolyte gradient. This is confirmed by Fig. 7(a) and (b) in Appendix A, where we compute the chemiphoretic and electrophoretic mobilities, and they are positive for the entire range of κa. In Fig. 5(a), the dashed line recovers the particle mobility in a free electrolyte solution.[18,59] The mobility increases as κa increases, since there are more ions contributing to stronger diffusiophoresis. The mobility plateaus in the limit of thin electric double layer, $\kappa a \gg 1$, due to the saturation of diffusioosmotic flux. The solid lines show the mobility in porous media with different permeabilities. At a fixed κa, lowering l/a decreases the magnitude of the mobility but does not change its sign, consistent with the explanation provided in Fig. 4.

Let us turn our focus to the lower quadrant of Fig. 5(a), which corresponds to a particle with $\hat{\zeta} = 1$. Recall from Fig. 4 that electrophoresis drives the particle down the electrolyte gradient and outweighs chemiphoresis that drives the particle up the electrolyte gradient. This is confirmed by Fig. 7(a) and (b) in Appendix A where, at particular l/a and κa, electrophoresis induces a negative mobility that has a larger magnitude relative to the positive mobility generated by chemiphoresis. In Fig. 5(a), the dashed line recovers the particle mobility in a free electrolyte solution.[18,59] As κa increases, the mobility decreases in magnitude and then plateaus. The solid lines show the mobility in porous media with different permeabilities. Notably, for $l/a < 1$, the magnitude of the diffusiophoretic mobility increases with κa monotonically, which is qualitatively different from that in a free electrolyte solution. This is due to the fact that porous media weaken the chemiphoretic and electrophoretic mobilities to different extents at different l/a and κa. Physically, this implies that particle diffusiophoresis in response to a change in the electrolyte concentration ($\kappa \sim \sqrt{n^{\infty}}$) in a porous medium could be qualitatively different from that in a free electrolyte solution.

Next, let us look at Fig. 5(b) that shows the variation of the non-dimensionalized diffusiophoretic mobility with κa for different κl. Let us first inspect the upper quadrant of the figure, which corresponds to a particle with a constant non-dimensionalized surface potential $\hat{\zeta} = -1$. The dashed line recovers the particle mobility in a free electrolyte solution.[18,59] The solid lines show the mobility in porous media with different κl. Compared to Fig. 3(b), the diffusiophoretic mobility still increases and then decreases with increasing κa, although this trend occurs only for $\kappa l > 1$ because of the electrophoretic contribution to the diffusiophoretic mobility. We show the chemiphoretic and electrophoretic mobility in Fig. 7(c) and (d) in Appendix A for reference. For $\kappa l \leq 1$, the diffusiophoretic mobility decreases monotonically as κa increases. The lower quadrant of the figure corresponds to a particle with $\hat{\zeta} = 1$. Due to a competition between chemiphoresis and electrophoresis, for all κl, the magnitude of the diffusiophoretic mobility decreases monotonically as κa increases.

Fig. 5(c) shows the variation of the non-dimensionalized diffusiophoretic mobility with κa for different l/a. The non-dimensionalized particle surface charge is fixed instead of the surface potential. The upper and lower quadrant of the figure correspond to a particle with $\hat{q} = -3.5$ and $\hat{q} = 3.5$, respectively. Although electrophoresis is present here, it only alters quantitatively the variation of the diffusiophoretic mobility with κa compared to that in a purely chemiphoretic system [Fig. 3(c)]. Specifically, regardless of the sign of the particle surface charge, the following trends persist. First, at a fixed κa, the magnitude of the mobility decreases as l/a decreases. Second, at a fixed l/a,

Published on 17 2023. Downloaded on 02.11.2024 23:21:51.

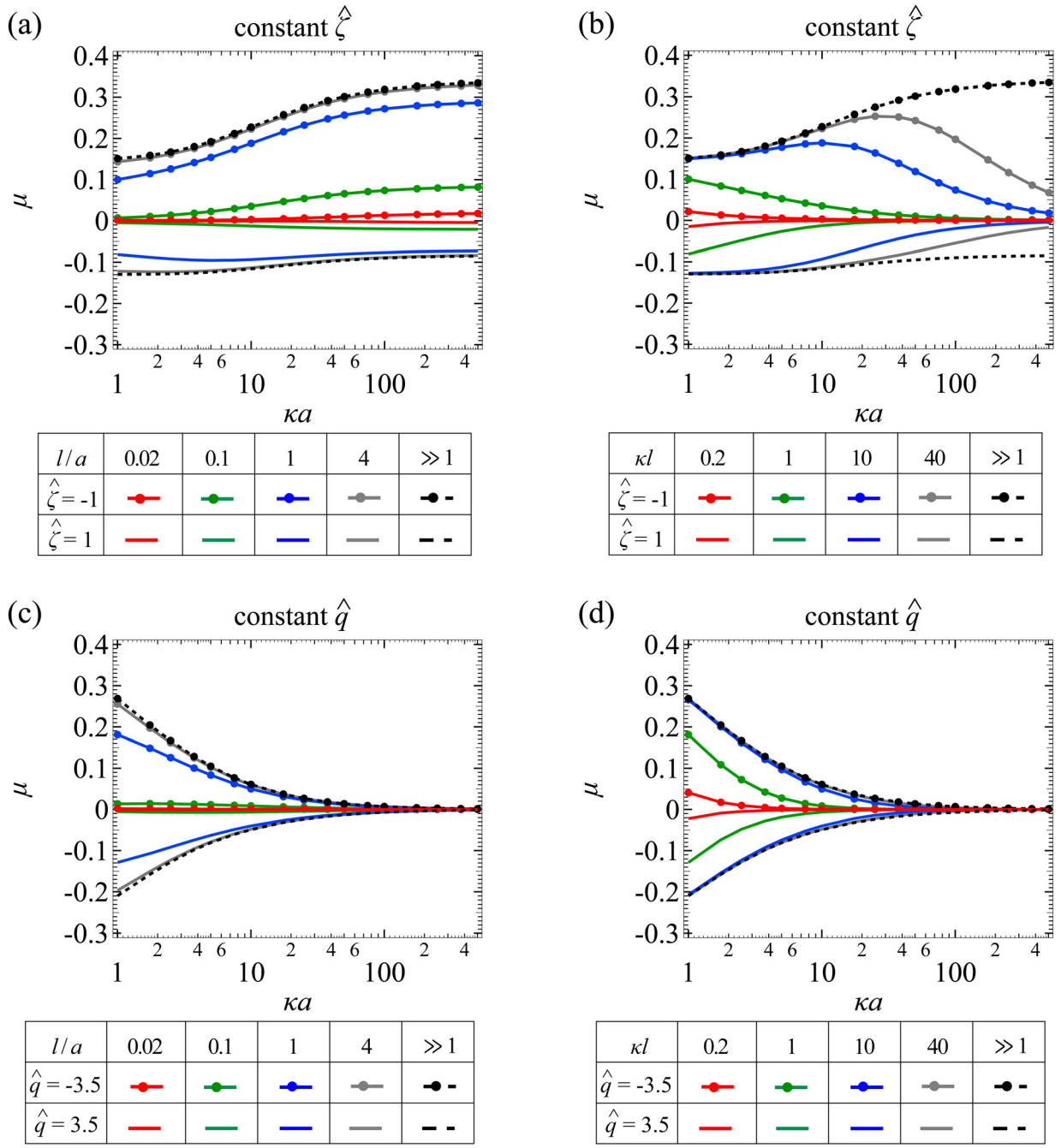

Fig. 5 Diffusiophoresis in porous media with sodium chloride solution where $\beta = -0.21$. (a) Variation of the non-dimensionalized diffusiophoretic mobility μ with the ratio of particle radius to Debye length κa for different ratios of Brinkman screening length to particle radius l/a. The non-dimensionalized particle surface potential $\hat{\zeta} = -1$ and 1 in the upper and lower quadrant, respectively. Dashed lines: a free electrolyte solution where $l/a \gg 1$. Solid lines: electrolyte-filled porous media of different l/a. (b) Variation of μ with κa for different ratios of Brinkman screening length to Debye length κl. $\hat{\zeta} = -1$ and 1 in the upper and lower quadrant, respectively. Dashed lines: a free electrolyte solution where $\kappa l \gg 1$. Solid lines: electrolyte-filled porous media of different κl. Parameters used in (c) and (d) are the same as (a) and (b), respectively, except that the non-dimensionalized particle surface charge $\hat{q}$ is fixed instead of the surface potential. $\hat{q} = -3.5$ and 3.5 in the upper and lower quadrant, respectively.

the mobility decreases monotonically to zero on approaching the limit $\kappa a \gg 1$.

Fig. 5(d) shows the variation of the non-dimensionalized diffusiophoretic mobility with κa for different κl. The upper and lower quadrant of the figure correspond to a particle with $\hat{q} = -3.5$ and $\hat{q} = 3.5$, respectively. Same as the conclusion drawn from Fig. 5(c), the presence of electrophoresis does not alter qualitatively the variation of the diffusiophoretic mobility compared to that in a purely chemiphoretic system [Fig. 3(d)]. At a fixed κa, the magnitude of the mobility decreases as κl decreases. At a fixed κl, the mobility decreases as κa increases.

 This journal is © The Royal Society of Chemistry 2023

Published on 17 2023. Downloaded on 02.11.2024 23:21:51.

3.3 Comparison with experiments

As noted in Section 1, recent experiments measured the nanoparticle diffusiophoretic mobility in porous media.[45] In this section, we compare our modeling predictions with experimental measurements. Before discussing the results, we state the justifications for the comparison. First, our model assumes a weak electrolyte concentration gradient, $|\nabla n_i^\infty/n_i^\infty|a \ll 1$. This condition is satisfied and can be confirmed by substituting relevant parameters from experiments as stated below. Second, our model computes the diffusiophoretic mobility of a single particle, excluding particle–particle hydrodynamic and electrostatic interactions. Neglecting these interactions is justified given the dilute particle suspension employed in experiments, since hydrodynamic disturbance and electric field due to a particle decay rapidly as $1/r^3$ and in an exponential manner, respectively.[58] Third, our model neglects particle interactions with physical confinements, *e.g.*, the dead-end pore walls in experiments. Neglecting this effect is justified so long as the particle is far from the confinement.

Fig. 6(a) shows the variation of the dimensional diffusiophoretic mobility with the concentration of the collagen gel (the porous medium). The collagen gel concentration, w, relates to the permeability *via* $l^2 = 30\,854w^{-1.442}$,[52] where the units for l and w in this relation are nm and mg mL^{-1}, respectively. In experiments,[45] a concentration gradient of potassium acetate of c_{in} = 1 mM to c_{out} = 0.025 mM over a distance of 800 μm is imposed to drive particles of radius 100 nm and surface potential 60 mV into a gel-filled dead-end pore. Utilizing these experimental parameters, we compute the mobilities with our model (line) and show them alongside the experimental measurements (circle). Our model predictions capture the experimental data qualitatively, where increasing the collagen concentration decreases the mobility due to the larger hydrodynamic drag to particle. Furthermore, our model predictions are in close quantitative agreement with experiments. We attribute the discrepancy to the large particle surface potential, 60 mV, which violates the range of validity of the Debye–Huckel approximation in our model formulation, namely, $|\zeta| \leq 50$ mV at room temperature.[54]

Fig. 6(b) shows the variation of the dimensional diffusiophoretic mobility with the particle radius. In experiments,[45] a concentration gradient of NaCl of c_{in} = 150 mM to c_{out} = 15 mM over a distance of 800 μm is imposed to drive particles of surface potential −21 mV into a gel-filled dead-end pore. The gel concentration is 2.4 mg mL^{-1}. Again, utilizing these experimental parameters, we compute the mobilities with our model (line) and show them alongside the experimental measurements (circle). Since the particle potential is within the range of validity of the Debye–Huckel approximation, here our model predictions match excellently with experiments. We propose an explanation for the discrepancy between our model and experiments in the two data points on the right as follows. As noted in experiments,[45] the significantly lower mobility of the two data points may be due to the strong particle-gel interactions. Specifically, although the net charge of the gel was reported as zero in experiments, we conjecture that any residue net charge of the gel will alter the electric potential distribution around the charged particle, which may in turn lower the particle mobility.[57,58] This effect is weak when the particle is small compared to the gel mesh but is more prominent when the two are comparable in size. Also, a charged gel will induce diffusioosmosis, which will alter the particle mobility in a non-trivial manner. Note that accounting for these effects requires a significant extension of the present model, including modification of the Poisson equation, the induced electric potential gradient, and consideration of a diffusioosmotic flow generated by porous media, which is beyond the scope of this work on particle diffusiophoresis in uncharged porous media but warrants future work.

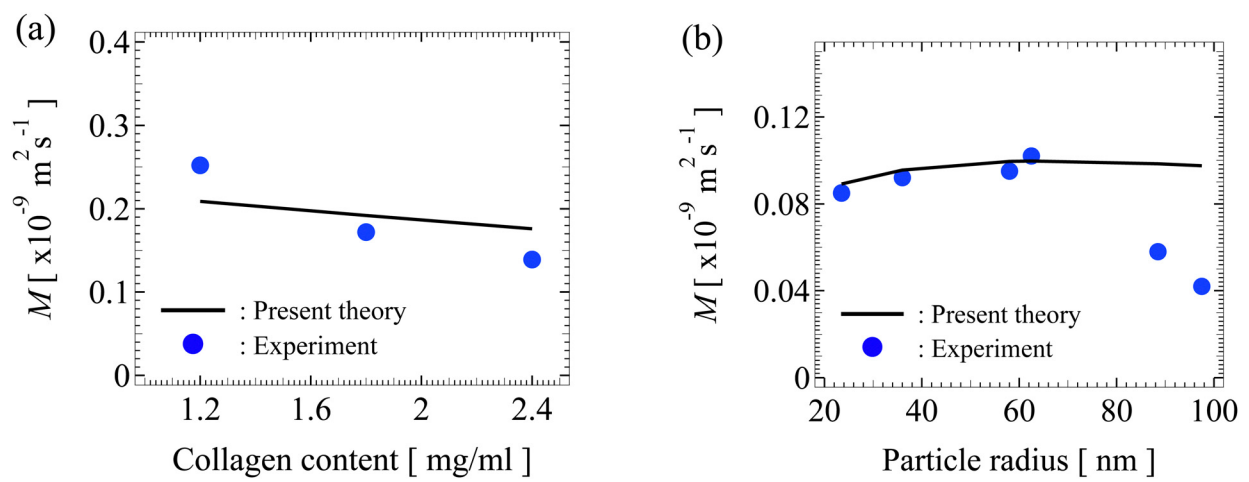

Fig. 6 (a) Variation of the dimensional diffusiophoretic mobility M with the concentration of the collagen gel. A concentration gradient of potassium acetate of c_{in} = 1 mM to c_{out} = 0.025 mM over a distance of 800 μm is imposed to drive particles of radius a = 100 nm and surface potential 60 mV into a gel-filled dead-end pore. (b) Variation of M with a. A concentration gradient of sodium chloride of c_{in} = 150 mM to c_{out} = 15 mM over a distance of 800 μm is imposed to drive particles of surface potential −21 mV into a gel-filled dead-end pore. The gel concentration is 2.4 mg mL^{-1}. Solid line: predictions by present work. Circle: experimental measurements by Doan *et al.*[45]

Published on 17 2023. Downloaded on 02.11.2024 23:21:51.

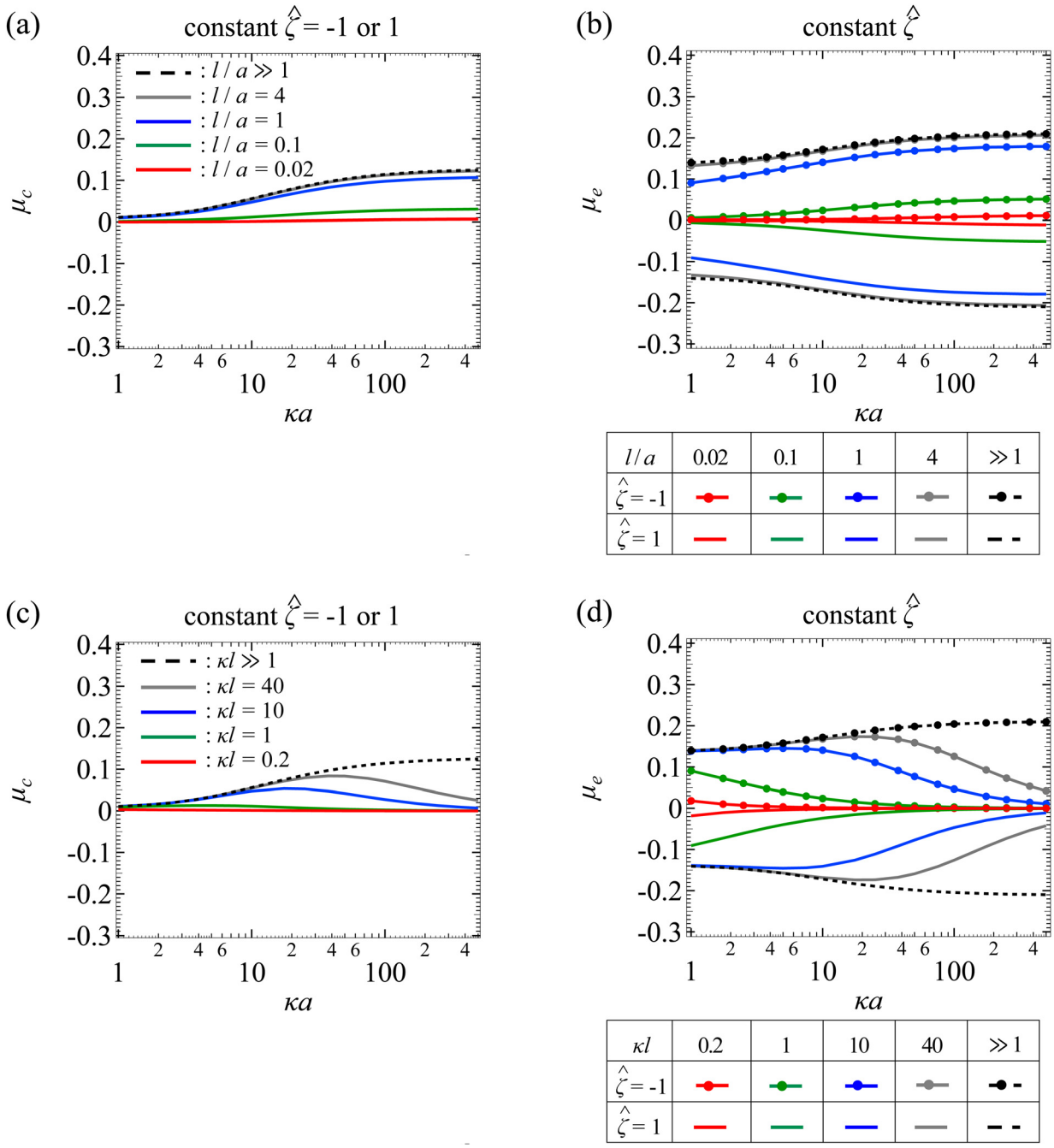

Fig. 7 Diffusiophoresis in porous media with sodium chloride solution where $\beta = -0.21$. Variation of (a) chemiphoretic μ_c and (b) electrophoretic μ_e component of the non-dimensionalized diffusiophoretic mobility μ with the ratio of particle radius to Debye length κa for different ratios of Brinkman screening length to particle radius l/a. For (a), results are the same for the non-dimensionalized particle surface potential $\hat{\zeta} = -1$ or 1. For (b), $\hat{\zeta} = -1$ and 1 in the upper and lower quadrant, respectively. Dashed lines: a free electrolyte solution where $l/a \gg 1$. Solid lines: electrolyte-filled porous media of different l/a. Variation of (c) μ_c and (d) μ_e with κa for different ratios of Brinkman screening length to Debye length κl. For (c), results are the same for $\hat{\zeta} = -1$ or 1. For (d), $\hat{\zeta} = -1$ and 1 in the upper and lower quadrant, respectively. Dashed lines: a free electrolyte solution where $\kappa l \gg 1$. Solid lines: electrolyte-filled porous media of different κl.

4 Conclusions

In this work, we have utilized the regular perturbation method to develop a mathematical model for predicting the diffusiophoretic mobility of a colloidal particle driven by a binary monovalent electrolyte concentration gradient in a porous medium. Our model is applicable to particles with surface potential $|\zeta| \leq 50$ mV at room temperature. To demonstrate our model, we have computed and analyzed the diffusiophoretic mobility of a particle in porous media filled with potassium chloride solution, where chemiphoresis dominates and

 This journal is © The Royal Society of Chemistry 2023

Published on 17 2023. Downloaded on 02.11.2024 23:21:51.

electrophoresis is negligible. We have shown that, compared to diffusiophoresis in a free electrolyte solution, the particle mobility could be significantly hampered in porous media due to additional hydrodynamic drag. Because of the absence of electrophoresis, the mobility is the same regardless of the sign of the particle surface charge. We have further computed and analyzed the diffusiophoretic mobility of a particle in porous media filled with sodium chloride solution, where chemiphoresis and electrophoresis both contribute to diffusiophoresis. The presence of porous media could still significantly weaken the particle mobility. However, since the chemiphoretic and electrophoretic components are weakened to different extents, the variation of the diffusiophoretic mobility with respect to a change in the electrolyte concentration in a porous medium could be qualitatively different from that in a free electrolyte solution.

We have also compared our model predictions with experiments and demonstrated excellent agreements within the scope of the model. There are discrepancies between our model predictions and experiments when assumptions of the model are violated, such as highly charged particles and charged porous media. This suggests future work to extend the present model to incorporate a net charge of the porous media and account for the modified, fully nonlinear Poisson–Boltzmann equation.

Conflicts of interest

There are no conflicts of interest to declare.

Appendix A: chemiphoretic and electrophoretic components of diffusiophoretic mobility in porous media with NaCl solution

Diffusiophoretic mobility, μ, could be expressed as a sum of its chemiphoretic, μ_c, and electrophoretic components, μ_e, that is, $\mu = \mu_c + \mu_e$. In Section 3.2, we utilized this fact to explain the variation of μ in Fig. 5(a) and (b). In this appendix, we discuss how we compute μ_c and μ_e, the variation of μ_c and μ_e, and that their sum indeed equals to μ.

Recall that μ_e arises from the electric field due to the difference in ion diffusivities, represented by the diffusivity ratio β. Terms that depend on β reside in eqn (25) only in the overall calculation of μ [solving eqn (19) and (20) subject to eqn (25), (27) and (28)]. Thus, we exploit the linearity of the equations[12,15] and separate eqn (25) into a part which depends on β and is associated with μ_e, and a part which does not depend on β and is associated with μ_c. In other words, μ_e can be calculated by replacing eqn (25) with

$$2\Psi_1^1 + R\frac{d\Psi_1^1}{dr} = 3\beta R, \quad 2\Psi_2^1 + R\frac{d\Psi_2^1}{dr} = 3\beta R, \tag{30}$$

and μ_c can be calculated by replacing eqn (25) with

$$2\Psi_1^1 + R\frac{d\Psi_1^1}{dr} = -3R, \quad 2\Psi_2^1 + R\frac{d\Psi_2^1}{dr} = 3R. \tag{31}$$

Fig. 7(a) shows the variation of μ_c with κa for different l/a. The physical interpretations are the same as Fig. 3(a) so we do not repeat them here. Fig. 7(b) shows the variation of μ_e with κa for different l/a. The upper and lower quadrant of the figure correspond to a particle with $\hat{\zeta} = -1$ and $\hat{\zeta} = 1$, respectively. As κa increases, the mobility increases in magnitude and then plateaus due to saturation of the electroosmotic flux in the limit $\kappa a \gg 1$. At a fixed κa, lowering l/a decreases the magnitude of the mobility due to the additional hydrodynamic drag by the porous media. Note that the mobility is symmetric with respect to the sign of the particle surface potential, that is, the mobility is symmetric about the κa axis. This is because of the fact that oppositely charged particles subject to the same electric field are driven into motion with the same speed but in the opposite direction. On a different note, when adding up μ_c and μ_e from Fig. 7(a) and (b), the result indeed recovers the diffusiophoretic mobility, μ, in Fig. 5(a), where Fig. 5(a) is obtained directly using eqn (25).

Fig. 7(c) shows the variation of μ_c with κa for different κl. The physical interpretations are the same as Fig. 3(b) so we do not repeat them here. Fig. 7(d) shows the variation of μ_e with κa for different κl. The upper and lower quadrant of the figure correspond to a particle with $\hat{\zeta} = -1$ and $\hat{\zeta} = 1$, respectively. The dashed lines correspond to the mobility in a free electrolyte solution. The mobility increases in magnitude and then plateaus due to saturation of the electroosmotic flux in the limit $\kappa a \gg 1$. The solid lines correspond to the mobility in porous media, which varies non-monotonically with κa. This is owing to the competition between the enhancement of the mobility due to the electroosmotic flux and the weakening of the mobility due to hindrance by the porous media. On a different note, at a fixed κa, lowering κl decreases the mobility, since this corresponds to lowering l/a and increasing hydrodynamic drag. By the same reasoning as Fig. 7(b), the mobilities in the two quadrants in Fig. 7(d) are equal in magnitude but opposite in sign. Finally, when adding up Fig. 7(c) and (d), the result indeed recovers the diffusiophoretic mobility, μ, in Fig. 5(b).

Acknowledgements

H. C. W. Chu acknowledges the startup funding support from the Division of Sponsored Programs, Department of Chemical Engineering, and Herbert Wertheim College of Engineering at University of Florida. We thank the anonymous referees for providing useful comments.

References

1 J. L. Anderson, *Annu. Rev. Fluid Mech.*, 1989, **21**, 61–99.
2 H. J. Keh, *Curr. Opin. Colloid Interface Sci.*, 2016, **24**, 13–22.

Published on 17 2023. Downloaded on 02.11.2024 23:21:51.

3 D. Velegol, A. Garg, R. Guha, A. Kar and M. Kumar, *Soft Matter*, 2016, **12**, 4686–4703.
4 S. Marbach and L. Bocquet, *Chem. Soc. Rev.*, 2019, **48**, 3102–3144.
5 D. C. Prieve, *Adv. Colloid Interface Sci.*, 1982, **16**, 321–335.
6 D. C. Prieve, J. L. Anderson, J. P. Ebel and M. E. Lowell, *J. Fluid Mech.*, 1984, **148**, 247–269.
7 J. F. Brady, *J. Fluid Mech.*, 2011, **667**, 216–259.
8 T. Chiang and D. Velegol, *J. Colloid Interface Sci.*, 2014, **424**, 120–123.
9 N. Shi, R. Nery-Azevedo, A. I. Abdel-Fattah and T. M. Squires, *Phys. Rev. Lett.*, 2016, **117**, 258001.
10 A. Gupta, B. Rallabandi and H. A. Stone, *Phy. Rev. Fluids*, 2019, **4**, 043702.
11 P. B. Warren, S. Shin and H. A. Stone, *Soft Matter*, 2019, **15**, 278–288.
12 H. Ohshima, *Colloid Polym. Sci.*, 2021, **299**, 1877–1884.
13 J. C. Baygents and D. A. Saville, *PhysicoChem. Hydrodyn.*, 1988, **10**, 543–560.
14 J. Lou and E. Lee, *J. Phys. Chem. C*, 2008, **112**, 12455–12462.
15 P. Y. Huang and H. J. Keh, *J. Phys. Chem. B*, 2012, **116**, 7575–7589.
16 W. Fang and E. Lee, *J. Colloid Interface Sci.*, 2015, **459**, 273–283.
17 F. Yang, S. Shin and H. A. Stone, *J. Fluid Mech.*, 2018, **852**, 37–59.
18 E. Lee, *Theory of electrophoresis and diffusiophoresis of highly charged colloidal particles*, Elsevier, New York, 2019.
19 S. Majhi and S. Bhattacharyya, *Colloids Surf., A*, 2022, **648**, 129272.
20 H. Ohshima, *Colloid Polym. Sci.*, 2022, **300**, 153–157.
21 P. Y. Chen and H. J. Keh, *J. Colloid Interface Sci.*, 2005, **286**, 774–791.
22 Y. C. Chang and H. J. Keh, *J. Colloid Interface Sci.*, 2008, **322**, 634–653.
23 H. C. Chiu and H. J. Keh, *Electrophoresis*, 2017, **38**, 2468–2478.
24 B. Abecassis, C. Cottin-Bizonne, C. Ybert, A. Ajdari and L. Bocquet, *New J. Phys.*, 2009, **11**, 075022.
25 J. Palacci, B. Abecassis, C. Cottin-Bizonne, C. Ybert and L. Bocquet, *Phys. Rev. Lett.*, 2010, **104**, 138302.
26 J. Deseigne, C. Cottin-Bizonne, A. D. Stroock, L. Bocquet and C. Ybert, *Soft Matter*, 2014, **10**, 4795–4799.
27 R. Volk, C. Mauger, M. Bourgoin, C. Cottin-Bizonne, C. Ybert and F. Raynal, *Phys. Rev. E: Stat., Nonlinear, Soft Matter Phys.*, 2014, **90**, 013027.
28 A. Banerjee, I. Williams, R. N. Azevedo, M. E. Helgeson and T. M. Squires, *Proc. Natl. Acad. Sci. U. S. A.*, 2016, **113**, 8612–8617.
29 C. Mauger, R. Volk, N. Machicoane, M. Bourgoin, C. Cottin-Bizonne, C. Ybert and F. Raynal, *Phy. Rev. Fluids*, 2016, **1**, 034001.
30 S. M. Friedrich, J. M. Burke, K. J. Liu, C. F. Ivory and T. Wang, *Nat. Commun.*, 2017, **8**, 1213.
31 V. Shukla, R. Volk, M. Bourgoin and A. Pumir, *New J. Phys.*, 2017, **19**, 123030.
32 F. Raynal, M. Bourgoin, C. Cottin-Bizonne, C. Ybert and R. Volk, *J. Fluid Mech.*, 2018, **847**, 228–243.
33 H. C. W. Chu, S. Garoff, R. D. Tilton and A. S. Khair, *Soft Matter*, 2020, **16**, 238–246.
34 T. J. Shimokusu, V. G. Maybruck, J. T. Ault and S. Shin, *Langmuir*, 2020, **36**, 7032–7038.
35 M. K. Rasmussen, J. N. Pedersen and R. Marie, *Nat. Commun.*, 2020, **11**, 2337.
36 H. C. W. Chu, S. Garoff, R. D. Tilton and A. S. Khair, *J. Fluid Mech.*, 2021, **917**, A52.
37 H. C. W. Chu, S. Garoff, R. D. Tilton and A. S. Khair, *Soft Matter*, 2022, **18**, 1896–1910.
38 R. E. Migacz and J. T. Ault, *Phy. Rev. Fluids*, 2022, **7**, 034202.
39 R. Volk, M. Bourgoin, C. Brehier and F. Raynal, *J. Fluid Mech.*, 2022, **948**, A42.
40 B. E. McKenzie, H. C. W. Chu, S. Garoff, R. D. Tilton and A. S. Khair, *J. Fluid Mech.*, 2022, **949**, A17.
41 N. Shi and A. Abdel-Fattah, *Phy. Rev. Fluids*, 2021, **6**, 053103.
42 H. Tan, A. Banejee, N. Shi, X. Tang, A. Abdel-Fattah and T. M. Squires, *Sci. Adv.*, 2022, **7**, eabh0638.
43 S. W. Park, J. Lee, H. Yoon and S. Shin, *Energy Fuels*, 2021, **35**, 4885–4892.
44 S. Shin, V. S. Doan and J. Feng, *Phys. Rev. Appl.*, 2019, **12**, 024014.
45 V. S. Doan, S. Chun, J. Feng and S. Shin, *Nano Lett.*, 2021, **21**, 7625–7630.
46 S. Shin, J. T. Ault, P. B. Warren and H. A. Stone, *Phys. Rev. X*, 2017, **4**, 041038.
47 H. Lee, J. Kim, J. Yang, S. W. Seo and S. J. Kim, *Lab Chip*, 2018, **18**, 1317–1724.
48 S. Shim, M. Baskaran, E. H. Thai and H. A. Stone, *Lab Chip*, 2021, **17**, 3387–3400.
49 A. Kar, T. Chiang, I. O. Rivera, A. Sen and D. Velegol, *ACS Nano*, 2015, **9**, 746–753.
50 S. Shin, E. Um, B. Sabass, J. T. Ault, M. Rahimi, P. B. Warren and H. A. Stone, *Proc. Natl. Acad. Sci. U. S. A.*, 2016, **113**, 257–261.
51 J. T. Ault, P. B. Warren, S. Shin and H. A. Stone, *Soft Matter*, 2017, **13**, 9015–9023.
52 S. Ramanujan, A. Pluen, T. D. McKee, E. B. Brown, Y. Boucher and R. K. Jain, *Biophys. J.*, 2002, **83**, 1650–1660.
53 M. Grossman, N. Ben-Chetrit, A. Zhuravlev, R. Afik, E. Bassat, I. Solomonov, Y. Yarden and I. Sagi, *Cancer Res.*, 2016, **76**, 4249–4258.
54 H. Ohshima, *Theory of colloid and interfacial electric phenomena*, Elsevier, New York, 2006.
55 H. C. Brinkman, *Appl. Sci. Res.*, 1947, **1**, 27–34.
56 S. A. Allison, Y. Xin and H. Pei, *J. Colloid Interface Sci.*, 2007, **313**, 328–337.
57 F. Li and R. J. Hill, *J. Colloid Interface Sci.*, 2013, **394**, 1–12.
58 R. J. Hill, *Soft Matter*, 2016, **12**, 8030–8048.
59 D. C. Prieve and R. Roman, *J. Chem. Soc., Faraday Trans. 2*, 1987, 1287–1306.
60 R. W. O'Brien and L. R. White, *J. Chem. Soc., Faraday Trans. 2*, 1978, 1607–1626.
61 R. W. O'Brien and R. J. Hunter, *Can. J. Chem.*, 1981, **81**, 1878–1887.

 This journal is © The Royal Society of Chemistry 2023

62 H. J. Keh and Y. K. Wei, *Langmuir*, 2000, **16**, 5289–5294.
63 R. F. Stout and A. S. Khair, *Phy. Rev. Fluids*, 2017, **2**, 014201.
64 R. J. Phillips, W. M. Deen and J. F. Brady, *AIChE J.*, 1989, **35**, 1761–1769.
65 A. Garg, C. A. Cartier, K. J. M. Bishop and D. Velegol, *Langmuir*, 2016, **32**, 11837–11844.
66 B. M. Alessio, S. Shim, E. Mintah, A. Gupta and H. A. Stone, *Phy. Rev. Fluids*, 2021, **6**, 054201.

Published on 17 2023. Downloaded on 02.11.2024 23:21:51.